Star Formation Sequence in a Hierarchical Universe

ChangHoon Hahn[1,2], Jeremy L. Tinker[2], Andrew R. Wetzel[3,4,5]

changhoon.hahn@lbl.gov

DRAFT --- 36a6894 --- 2018-08-28 --- NOT READY FOR DISTRIBUTION

ABSTRACT

motivation, methodology, impact. In observations star forming galaxies form a tight *log* M_* to *log* SFR relation referred to as the *star formation main sequence* (SFS) out to $z \sim 2$. Beyond the evolution "along" this SFS, however, the star formation histories of star forming galaxies have not been precisely characterized. The SFH of these galaxies govern SMF, SFS, and also observed constraints on the stellar mass to halo mass relation.

By combining high-resolution cosmological N-body simulation with observed evolutionary trends of SF galaxies, we construct a model that tracks the evolution of star forming central galaxies over the redshift $z < 1$. Comparing this model

Observations find a remarkably small scatter in the stellar mass to halo mass relation. Somehow the star formation histories of galaxies must

According to observations, star forming galaxies form a tight *log* M_* to *log* SFR relation referred to as the "star formation main sequence" out to $z \sim 2$.

Subject headings: methods: numerical – galaxies: clusters: general – galaxies: groups: general – galaxies: evolution – galaxies: haloes – galaxies: star formation – cosmology: observations.

1. Introduction

- Motivate why we think SF galaxies evolve along the main sequence
- Discuss the current thought process on galaxy assembly bias
- Explain the limitation of SFH derivable from observations (Claire's fisher matrix paper would be really good; ask her about the details)

[1]Lawrence Berkeley National Laboratory, 1 Cyclotron Road, Berkeley, CA 94720

[2]Center for Cosmology and Particle Physics, Department of Physics, New York University, 4 Washington Place, New York, NY 10003

[3]TAPIR, California Institute of Technology, Pasadena, CA USA

[4]Carnegie Observatories, Pasadena, CA USA

[5]Department of Physics, University of California, Davis, CA USA

- in fact we can't constrain sf variability very well even in simulations due to the time resolution (see Hahn et al. (in prep.)).
- Observations also can't provide detail host dark matter halo properties
- So the approach with combining observations with N-body (empirical modeling) is very effective in the context of the halo.
- Maybe talk about how the bigger context of why this is important?
- Why only centrals – because our current best understanding of satellites is that they quench after infall, so it doesn't make sense to look at them
- our model goes from $z < 1$ because beyond that the observations are statistically meaningless.

2. Central Galaxies of SDSS DR7

We construct our galaxy sample following the sample selection of Tinker et al. (2011). We select a volume-limited sample of galaxies with $M_r 5log(h) < 18$ and complete in $M_* > 10^{9.4} M_\odot$ from the NYU Value-Added Galaxy Catalog (VAGC; Blanton et al. 2005) of the Sloan Digital Sky Survey Data Release 7 (SDSS DR7; Abazajian et al. 2009) at $z \approx 0.04$. The stellar masses of these galaxies are estimated using the `kcorrect` code (Blanton & Roweis 2007) assuming a Chabrier (2003) initial mass function. The star formation of the galaxies are estimated spectroscopically using the specific star formation rates (SSFR) from the current release of the MPA-JHU spectral reductions[1] (Brinchmann et al. 2004). Generally speaking, SSFR $> 10^{-11}\mathrm{yr}^{-1}$ are derived from H_α emission, $10^{-11} >$ SSFR $> 10^{-12}\mathrm{yr}^{-1}$ are derived from a combination of emission lines, and SSFR $< 10^{-12}\mathrm{yr}^{-1}$ are based on D_n4000 (see discussion in Wetzel et al. 2013). We note that SSFR $< 10^{-12}\mathrm{yr}^{-1}$ should only be considered upper limits to the true galaxy SSFR (Salim et al. 2007).

From our galaxy sample, we identify the central galaxies using the Tinker et al. (2011) halo-based group-finding algorithm, which is based on the Yang et al. (2005) algorithm and tested in Campbell et al. (2015). The algorithm assigns a probability of being a satellite, $P_{\rm sat}$, to each galaxy in the sample. Galaxies with $P_{\rm sat} \geq 0.5$ are classified as satellites and $P_{\rm sat} < 0.5$ are classified as centrals. In this paper we focus on central galaxies. With any group finding algorithm, galaxies are misassigned due to projection effects and redshift space distortions. The purity of the full central galaxy sample is $\sim 90\%$ with a completeness of $\sim 95\%$ (Tinker et al. 2017a). Furthermore, Campbell et al. (2015) find that the algorithm

[1] http://wwwmpa.mpa-garching.mpg.de/SDSS/DR7/

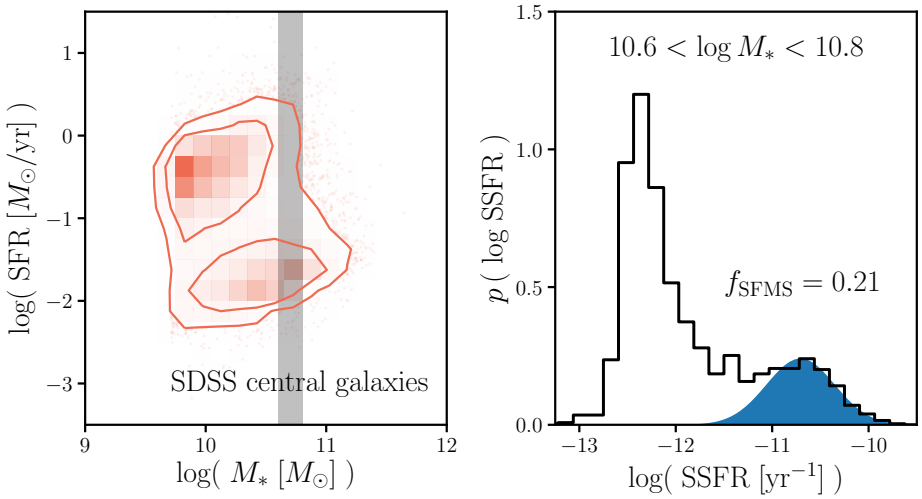

Fig. 1.— Central galaxies of the SDSS DR7 group catalog. *Left:* We plot the SFR-M_* relation of the SDSS central galaxies. The contours illustrate the bimodal distribution of the galaxy properties and mark the star-forming and quiescent populations. The transitioning galaxies lie on the "green" valley between the star-fomring and quiescent modes. *Right:* We plot the distribution of $\log$ SSFR for SDSS centrals with $10.6 < \log M_* < 10.8$. Shaded in blue, we plot the SFS component of our GMM fit of the SFR-M_* relation described in Section 3.1. Based on this fit, galaxies in the SFS account for approximately $f_{\rm SFS} = 0.21$ of the central galaxies in the stellar mass bin.

robustly identifies red and blue centrals as a function of stellar mass, which is highly relevant to our analysis.

In the left panel of Figure 1, we plot the SFR-M_* distribution of the SDSS DR7 central galaxies. In the right panel, we plot the distribution of SSFR, $p(\log \mathrm{SSFR})$, for galaxies with $10.6 < \log M_* < 10.8$ (stellar mass range highlighted on the left panel). Both panels of Figure 1 illustrate the bimodality in the galaxy sample. The SFR-M_* distribution also illustrate the correlation between SFR and M_* in star-forming galaxies *i.e.* the star-formation main sequence (SFS).

3. Model: Simulated Central Galaxies

We're interesting in constructing a model that tracks central galaxies and their star formation within the heirarchical growth of their host halos. This requires a cosmological N-body simulation that accounts for the complex dynamical processes that govern the host halos of galaxies. In this paper we use the high resolution N-body simulation from Wetzel et al. (2013) generated using the White (2002) `TreePM` code with flat ΛCDM cosmology ($\Omega_m = 0.274, \Omega_b = 0.0457, h = 0.7, n = 0.95, \mathrm{and} \sigma_8 = 0.8$). From initial conditions at $z = 150$ generated from second-order Lagrangian Perturbation Theory, 2048^3 particles with mass of $1.98 \times 10^8\, M_\odot$ are evolved in a $250\mathrm{Mpc}/h$ box with a Plummer equivalent smoothing of $2.5\,\mathrm{kpc}/h$. For a more detailed description of the simulation, we refer readers to Wetzel et al. (2013, 2014).

From the TreePM N-body simulation, 'host halos' are identified using the Friends-of-Friends (FoF) algorithm of Davis et al. (1985) with linking length of $b = 0.168$ times the mean inter-partcile spacing. Within these host halos, Wetzel et al. (2013) identifies 'subhalos' as overdensities in phase space through a six-dimensional FoF algorithm (FoF6D White et al. 2010). The host halos and subhalos are then tracked across the simulation outputs from $z = 10$ to 0 to build merger trees (Wetzel et al. 2009; Wetzel & White 2010). The most massive subhalos in newly-formed host halos at a given simulation output are defined as the 'central' subhalo. A central subhalo retains its 'central' definition until it falls into a more massive host halo, at which point it becomes a 'satellite' subhalo.

At a given snapshot, we assign stellar masses used only for initializing our model to each subhalo by subhalo abundance matching (SHAM; Conroy et al. 2006; Vale & Ostriker 2006; Yang et al. 2009; Wetzel et al. 2012; Leja et al. 2013; Wetzel et al. 2013, 2014; **?**) to M_{peak}, the maxmum host halo mass that it ever had as a central subhalo. SHAM, in its simplest form, assumes a one-to-one mapping between subhalo M_{peak} and galaxy stellar mass M_* that preserves rank order: $n(> M_{\mathrm{peak}}) > n(> M_*)$. In practice, we apply a 0.2 dex log-normal scatter in M at fixed M_{peak} based on the observed stellar to halo mass relation (SHMR; **bunch of SMHMR citations**). For $n(> M_*)$, we use observed stellar mass functions (SMFs) at the redshift corresponding to the snapshot. At $z = 0.05$, the lowest redshift

snapshot of our model, we use the SMF from Li & White (2009), which is based on the same SDSS NYU-VAGC sample as our group catalog. At higher redshifts, we interpolate between the Li & White (2009) SMF and the SMF from Marchesini et al. (2009) at $z = 1.6$. We choose the Marchesini et al. (2009) SMF, among others, because it produces interpolated SMFs that monotonically increase at $z < 1$. As noted in **?**, at $z \approx 1$, the SMF interpolated between the Li & White (2009) and Marchesini et al. (2009) SMFs is consistent with more recent measurements from Muzzin et al. (2013) and Ilbert et al. (2013). **TBD: Perhaps mention in appendix how we test different SMF assumptions**

Throughout its 45 snapshot outs, `TreePM` simulation tracks the evolution of subhalos back to $z \sim 10$. We restrict ourselves to 15 snapshots from $z = 1.08$ to $z = 0.05$, where we have the most statistically meaningful observations. Furthermore, since we're interested in centrals we only keep subhalos that are classified as centrals throughout the redshift range. This criterion removes "black splash" or "ejected" satellite galaxies (*e.g.* Mamon et al. 2004; Wetzel et al. 2014) misclassified as centrals. Finally, we have a model based on the `TreePM` N-body simulation that tracks the evolution of central subhalos from $z = 1.08$ to $z = 0.05$. Next, we describe how we select and initialize the star forming central galaxies from the central subhalos in our model.

3.1. Selecting Star Forming Centrals

In our model, we're interested in tracking the SFR and stellar mass evolution of SF central galaxies. To construct such a model, we first need to select SF galaxies from the central galaxies in our simulation, described above. Since we want our model to reproduce observations, our selection is based on $f_{\rm SFS}^{\rm cen}(M_*)$, the fraction of central galaxies within the star forming sequence, measured from the SDSS DR7 VAGC (Section 2). Below, we describe how we derive this $f_{\rm SFS}^{\rm cen}(M_*)$ and use it to select SF central galaxies in our model. Afterwards we describe how we initalize the SFRs and M_* of these galaxies in our model.

Often in the literature, an empirical color-color or SFR–M_* cut that separates the two main modes (red/blue or star-forming/quiescent) in the distribution is chosen to classify galaxies (*e.g.* Baldry et al. 2006; Blanton & Moustakas 2009; Drory et al. 2009; Peng et al. 2010; Moustakas et al. 2013; Hahn et al. 2015). The red/quiescent or blue/star-forming fractions derived from this sort of classification, by construction, depend on the choice of cut and neglect galaxy subpopulations such as transitioning galaxies *i.e.* galaxies in the "green valley". Instead, for our $f_{\rm SFS}^{\rm cen}(M_*)$, we use the SFS fitting method from Hahn et al. (in prep.). Hahn et al. (in prep.)uses Gaussian Mixture Models and the Bayesian Information Criteria in order to fit the SFR–M_* relation of a galaxy population and identify its SFS. This data-driven approach relaxes many of the assumptions and hard cuts that go into other methods. Furthermore, as they demonstrate in Hahn et al. (in prep.)by applying to multiple simulations, it can be flexibly applied to a wide range of star formation and M_*. The weight

of the SFS GMM component from the fitting provides an estimate of $f_{\rm SFS}^{\rm cen}$. In the right panel of Figure 1, we plot the SFS GMM component (blue shaded region) of the $p(\log {\rm SSFR})$ for the SDSS DR7 central galaxies within $10.6 < \log M_* < 10.8$. The SFS constitutes $f_{\rm SFS}^{\rm cen} = 0.21$ of the SDSS central galaxies in this stellar mass bin.

Rather than using the $f_{\rm SFS}^{\rm cen}$ values directly, for selecting SF galaxies, we fit $f_{\rm SFS}^{\rm cen}$ as a linear function of $\log M_*$ similar to Wetzel et al. (2013); Hahn et al. (2017a). We derive the following best-fit:

$$f_{\rm SFS,bestfit}^{\rm cen}(M_*) = -0.627\,(\log\, M_* - 10.5) + 0.354. \quad (1)$$

We note that this $f_{\rm SFS,bestfit}^{\rm cen}(M_*)$ is in good agreement with the $f_{\rm Q}^{\rm cen}(M_*; z\sim 0)$ fit from **?**. For each central galaxy in our simulation, we assign a probability of it being on the SFS, using Eq. 1 with M_* at $z\sim 0$ assigned through SHAM. Based on these probablities, we randomly identify centrals from our simulation as SF at $z\sim 0$. In our model, we make the assumption that once a SF galaxy quenches its star formation, it remains quiescent. Without any quiescent galaxies rejuvenating their star formation, galaxies on the SFS at $z\sim 0$ are also on the SFS at $z > 0$. Using this assumption the SF centrals we select at $z\sim 0$ are also on the SFS at the intial redshift of our model: $z\sim 1$.

Next, we can initialize the SF centrals at $z\sim 1$ using SHAM M_*s and assign their initial SFRs based on the observed SFR-M_* relation of the SFS. Observations in the literature at these redshifts, however, not only use galaxy properties derived differently from the SDSS VAGC but they also find SFS with significant discrepancies from one another. Speagle et al. (2014) compiles the SFR-M_* relation of the SFS from 25 studies in the literature, each with different methods of deriving galaxy properties. Even *after* their calibration, for a fixed $M_* = 10^{10.5}\,M_\odot$, the SFRs of the SFSs at $z\sim 1$ vary by more than a factor of 2 (see Figure 2 of Speagle et al. 2014). With little consensus on the SFS at $z\sim 1$, and consequently its redshift evolution, we flexibly parameterize the SFS SFR ($\log {\rm SFR}_{\rm MS}(M_*, z)$) with free parameters m_{M_*} and m_z that characterize the stellar mass and redshift dependences respectively. We parameterize the mean log SFR of the SFS as,

$$\log \overline{\rm SFR}_{\rm SFS}(M_*, z) = m_{M_*} * (\log\, M_* - 10.5) + m_z * (z - 0.05) - 0.11. \quad (2)$$

We assign SFRs to our SF centrals at $z\sim 1$ by sampling a log-normal distribution centered about $\log \overline{\rm SFR}_{\rm MS}(M_*, z = 1)$ with a constant scatter of 0.3 dex, motivated from observations (Daddi et al. 2007; Noeske et al. 2007; Magdis et al. 2012; Whitaker et al. 2012). Later in our analysis, for the priors of our parameters m_{M_*} and m_z, we conservatively choose a range that encompass the best-fit SFS from Speagle et al. (2014) and measurements from Moustakas et al. (2013) and Lee et al. (2015). With our SF centrals initalized at $z\sim 1$, next, we describe how we evolve their SFR and M_*.

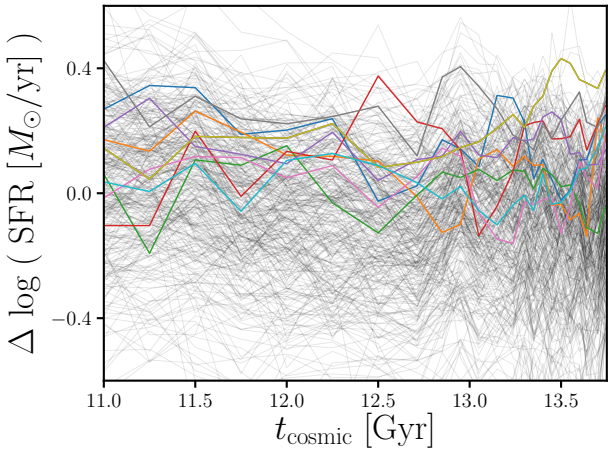

Fig. 2.— Star formation rate with respect to the log $\overline{\rm SFR}_{\rm SFS}$—$\Delta$ log SFR)—as a function of cosmic time for star-forming galaxies in the Illustris simulation. These galaxies have stellar masses within the range $10^{10.5} - 10^{10.6} M_\odot$ at $z \sim 0$. log $\overline{\rm SFR}_{\rm SFS}$ is fit using the Hahn et al. (in prep.)SFS fitting method, the same method we use for our SDSS centrals in Section 3.1. As the Δ log SFR(t)s in color emphasize how the SFRs of Illustris star-forming galaxies fluctuate about the mean SFS. *The* SFR *variability in the SFHs of SF centrals in our model (see Section 3.2) is motivated by this* Δ log SFR(t) *behavior in Illustris.*

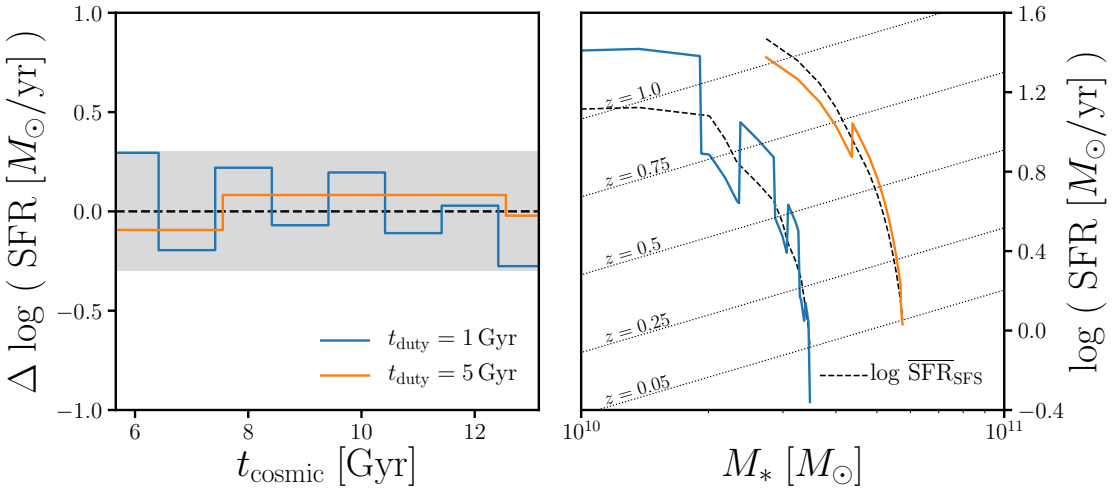

Fig. 3.— *Left*: The Δ log SFR evolution of two SF centrals using the fiducial model that incorporates star formation variability through a "star formation duty cycle" on two timescales $t_{\rm duty} = 1$ Gyr (blue) and 5 Gyr (orange). Δ log SFR(t)s determine the SFHs (Eq. 3), hence it also determines the M_* growth of the SF central galaxies in our model (Eq. 4). *Right*: The SFR$_i$ and $M_{*,i}$ evolutions of the same two SF central galaxies in our fiducial model with $t_{\rm duty} = 1$ Gyr (blue) and 5 Gyr (orange). For reference we plot log $\overline{\rm SFR}_{\rm SFS}(M_{*,i}(t), t)$ for each galaxy (black dashed) and log $\overline{\rm SFR}_{\rm SFS}(M_*)$ at various redshifts between $z = 1$ to 0.05 (dotted lines). As the SFR$_i$ and $M_{*,i}$ evolutions illustrate, *the SF centrals in our model evolve as their SFRs fluctate about the SFS.*

3.2. Evolving along the Star Formation Sequence

The tight correlation between the SFRs and stellar masses of SF galaxies (the so-called SFS) has been observed to span over four orders of magnitude in stellar mass and extends beyond the local universe out to $z > 2$ (*e.g.* Noeske et al. 2007; Daddi et al. 2007; **?**; Salim et al. 2007; Santini et al. 2009; Karim et al. 2011; Whitaker et al. 2012; Moustakas et al. 2013; Lee et al. 2015; see also references in Speagle et al. 2014). Even in hydrodynamic simulations and semi-analytic models, we find well defined SFSs (see Hahn et al. (in prep.)and references therein). The SFRs of galaxies on the SFS, for a given stellar mass follow a log-normal distribution with a roughly constant scatter (~ 0.3 dex in observations). Given its persistence in the local Universe, the SFS provides a anchoring relationship to characterize the SFRs and M_*s of SF galaxies throughout $z < 1$. More specifically, *we can characterize the star formation histories (SFHs) of our SF centrals with respect to the mean* log SFR *of the SFS* (Eq. 2):

$$\log \mathrm{SFR}(M_*, t) = \log \overline{\mathrm{SFR}}_{\mathrm{MS}}(M_*, t) + \Delta \log \mathrm{SFR}(t). \tag{3}$$

Since SFHs determine the M_* growth of galaxies, Δ log SFRs in our model dictate the SFHs and M_* evolution of SF centrals. Below, we describe the prescription for our fiducial $\Delta \log \mathrm{SFR}(t)$.

One naive example for $\Delta \log \mathrm{SFR}(t)$ would be to keep Δ log SFR fixed from the initial offsets from the log $\overline{\mathrm{SFR}}_{\mathrm{SFS}}$ in the initial SFRs of our SF central galaxies at $z \sim 1$. SF centrals with higher than average initial SFRs continue evolving above the average SFS, while SF centrals with lower than average initial SFRs continue evolving below the average SFS. In addition to the fact that such a SFH cannot reproduce observations, which we later demonstrate, we do not find such a SFH in SF galaxies of hydrodynamic simulations such as Illustris Vogelsberger et al. (2014); Genel et al. (2014). In Figure 2, we plot Δ log SFRs of SF galaxies in Illustris as a function of cosmic time. These galaxies have stellar masses within $10^{10.5} - 10^{10.6} M_\odot$ at $z = 0$. At each simultation output, we derive log $\overline{\mathrm{SFR}}_{\mathrm{SFS}}$ using the same Hahn et al. (in prep.)fitting method as in Section 3.1 and use it to calculate Δ log SFR (Eq. 3). As the Δ log SFRs highlighted in color illustrate, the $\Delta \log \mathrm{SFR}(t)$s of SF galaxies do not remain constant, but rather vary about the SFS.

Motivated by the $\Delta \log \mathrm{SFR}(t)$ of Illustris galaxies, we introduce variability in the SFHs of our SF centrals in the form of a "*star formation duty cycle*". We parameterize Δ log SFR to flucutate about the mean SFS on some duty cycle timescale t_{duty} with amplitude randomly sampled from a log-normal distribution with 0.3 dex scatter at every t_{duty} timestep. The full SFH of the SF centrals follow Eq. 3. In the left panel of Figure 3, we present $\Delta \log \mathrm{SFR}(t)$ of SF centrals with our fiducial star formation duty cycle prescription. The two $\Delta \log \mathrm{SFR}(t)$s have $t_{\mathrm{duty}} = 1$ Gyr (blue) and 5 Gyr (orange). The shaded region represents the observed 0.3 dex 1σ scatter of the SFS SFR. Although, we do not expect such a simplified model to reflect the exact individual SFHs of SF centrals, for the SF population it captures the

stochasticity from gas accretion, star-bursts, and feedback mechanisms. Furthermore, it allows us to measure the timescale of such variabilities. Also this Δ log SFR prescription by construction reproduces the observed log-normal SFR distribution of the SFS at any point in the model.

Next using our Δ log SFR prescription, we now evolve both the SFR and M_* of our SF centrals along the SFS. Based on Eq. 3, the SFRs of our SF centrals are functions of M_*. Meanwhile, M_* is the integral of the SFR over time:

$$M_*(t) = f_{\rm retain} \int_{t_0}^{t} \mathrm{SFR}(\mathrm{M_*, t})\, \mathrm{d}t + M_0. \tag{4}$$

t_0 and M_0 are the initial cosmic time and stellar mass at $z \sim 1$, respectively. $f_{\rm retain}$ here is the fraction of stellar mass that is retained after supernovae and stellar winds; we use $f_{\rm retain} = 0.6$ (Wetzel et al. 2013). By solving the differential equation from combining Eqs. 3 and 4, we evolve the SFR and M_* of our SF centrals. The right panel of Figure 3 presents the SFR_i and $M_{*,i}$ evolutions for the two SF centrals with different $t_{\rm duty}$ timescales in the left panel. For reference, we include log $\overline{\mathrm{SFR}}_{\rm SFS}(M_{*,i}(t), t)$ (black dashed) and log $\overline{\mathrm{SFR}}_{\rm SFS}(M_*)$ (dotted lines) at various redshifts between $z = 1$ to 0.05. As Figure 3 illustrates, using our Δ log SFR prescription the SF centrals evolve as their SFRs fluctuate along the SFS throughout the timesteps of our model.

We continue to evolve our SF central galaxies until the final $z = 0.05$ snapshot. For the SF centrals in our model, not only do we have SFRs and M_*s that we evolved but we also have their host halo properties from the `TreePM` N-body simulation. Using these properties, we can compare our model to observations and constrain the free parameters using observables such as the quiescent fraction and SMF. Once we have a model that reproduces the standard observables we can use the host halo properties to examine observables such as the SHMR. Next, we present this comparison between our model and observations and present the constraints we derive on the role and timescale of star formation variability in the evolution of SF galaxies.

4. Results

Our model takes `TreePM` central subhalos and tracks their SFR and M_* evolution using a flexible parameterization of the SFS and SFHs that incorporate variability through a star formation duty cycle. At $z = 0.05$, its final timestep, our model provides properties such as the SFR, M_*, and host halo mass, M_h, of central galaxies it classifies as SF. We now use these resulting properties to compare our model to observations and constrain its free parameters—the parameters of the Eq. 2 SFS. Since the focus of our model and this paper is on SF centrals, the main observable we use is the SMF of star forming centrals in SDSS,

which we estimate as

$$\Phi^{\rm SDSS}_{\rm SF,cen} = f^{\rm cen}_{\rm SFS} \times f_{\rm cen} \times \Phi^{\rm Li\&White(2009)}. \quad (5)$$

$f^{\rm cen}_{\rm SFS}$ is the fraction of central galaxies on the SFS, which we fit in Eq. 1. $f_{\rm cen}$ is the central galaxy fraction from Wetzel et al. (2013) and $\Phi^{\rm Li\&White(2009)}$ is the SMF of the SDSS from Li & White (2009). If our model reproduces the observed $\Phi^{\rm SDSS}_{\rm SF,cen}$, by construction, it also reproduces the observed quiescent fraction.

For the actual comparison of our model to observation, we use the parameter estimation framework of Approximate Bayesian Computation (ABC). ABC has the advantage over standard approaches to parameter inference in that it does not require evaluating the likelihood. It relies only on a simulation of the observed data and a distance metric to quantify the "closeness" between the observed data and simulation. Many variations of ABC has been used in astronomy and cosmology (*e.g.* **???**Alsing et al. 2018). We use ABC in conjunction with the efficient Population Monte Carlo (PMC) importance sampling as in (**?**Hahn et al. 2017a). For initial range of our ABC particles, *i.e.* the priors of our Eq. 2 SFS parameters A_z **and** m_z, we use uniform distributions spanning the ranges **numbers** and **numbers**, respectively. As we mentioned in Section 3.1, the range of the prior were conservatively chosen to encompass the best-fit SFS from Speagle et al. (2014) and measurements from Moustakas et al. (2013) and Lee et al. (2015) at $z \sim 1$. Finally, for our distance metric, we formulate a distance between the SMF of the SF centrals in our model to the observed $\Phi^{\rm SDSS}_{\rm SF,cen}$ (Eq. 5):

$$\rho_\Phi = \sum_M \left(\frac{\Phi^{\rm sim} - \Phi^{\rm SDSS}_{\rm SF,cen}}{\sigma'_\Phi} \right)^2. \quad (6)$$

$\Phi^{\rm sim}(M)$ is the SMF of the SF centrals in our model and $\sigma'_\Phi(M)$ **is the SMF uncertainty derived using mock catalogs from Li & White (2009)**. For the rest of our ABC-PMC implementation, we strictly follow the implementation of Hahn et al. (2017b) and **?**. We refer reader to those papers for further details.

4.1. The Star Formation Duty Cycle

In Figure 4, we present the SMFs (left), SFSs (middle), and $\sigma_{\log M_*}(\log M_{\rm halo})$ (right) of two models with different SFH prescriptions each run using the medians parameter values of their ABC posterior distributions — $\theta_{\rm median}$. One model has duty cycle of $t_{\rm duty} = 10\,{\rm Gyr}$ (red) while the other has a duty cycle of $t_{\rm duty} = 1\,{\rm Gyr}$ (blue). Both models, as expected from the ABC posteriors, successfully reproduce the SDSS SMF ($\Phi^{\rm SDSS}_{\rm SF,cen}$). By construction, *i.e.* the priors, they also have SFSs consistent with observations. Despite their consistency, however, *the difference in the star formation duty cycle timescales of the models results in dramatically different scatter in* $\log M_*$ *at a given* $\log M_{\rm halo}$ *(*i.e. *scatter in the SHMR)*, particularly below $M_{\rm halo} < 10^{12.5} M_\odot$.

Since the scatter in SHMR of our model depends on the star formation duty cycle timescale, we can compare the scatter from our model to observational constraints on the SHMR in order to constrain the star formation duty cycle and the SFHs of star forming galaxies (Figure 5). More specifically, in Figure 5, we present $\sigma_{\log M_*}$, the scatter in log M_* at fixed halo mass, at $M_h = 10^{12} M_\odot$) and $\sigma_{\log M_h}$, the scatter in log M_h at fixed stellar mass, at $M_* = 10^{10} M_\odot$ as a function of $t_{\rm duty}$ (left and right panels). For $t_{\rm duty}$ ranging from 10 to 0.5 Gyr, $\sigma_{\log M_*}$ ranges from $0.32^{+5.1}_{-4.0}$ **to** $0.26^{+5.1}_{-4.0}$ dex **and** $\sigma_{\log M_h}$ **ranges from number to number**. With a shorter star formation duty timescale, our model produces significantly smaller scatter in the SHMR.

In order to constrain $t_{\rm duty}$, we compare $\sigma_{\log M_*}$ and $\sigma_{\log M_h}$ in our model to observational constraints from the literature. These constraints are mainly derived from fitting some sort of halo occupation based models to observations of galaxy clustering, SMF, satellite kinematics, or galaxy-galaxy weak lensing. On the left panel, we include $\sigma_{\log M_*}$ constraints from More et al. (2011); Leauthaud et al. (2012); Tinker et al. (2013); Zu & Mandelbaum (2015). More et al. (2011); Zu & Mandelbaum (2015) fit satellite kinematics, galaxy clustering, and galaxy-galaxy lensing measurements of the SDSS VAGC. Meanwhile Leauthaud et al. (2012); Tinker et al. (2013) fit the SMF, galaxy clustering, and galaxy-galaxy lensing to COSMOS. Although, Leauthaud et al. (2012); Zu & Mandelbaum (2015) measure $\sigma_{\log M_*}$ for all central galaxies, at $M_h \sim 10^{12} M_\odot$ there is a $< 1\sigma$ difference in $\sigma_{\log M_*}$ between star-forming and quiescent central galaxies (More et al. 2011; Tinker et al. 2013). Hence we include them in Figure 5.

On the right panel, we include $\sigma_{\log M_h}$ constraints from More et al. (2011) along with constraints from Mandelbaum et al. (2006b); Conroy et al. (2007); Velander et al. (2014); Han et al. (2015). Mandelbaum et al. (2006b); Velander et al. (2014) use halo occupation models to analyze galaxy-galaxy weak lensing measurements of SDSS and CFHTLenS**cite**, respectively. Conroy et al. (2007), similar to More et al. (2011), use halo model to fit the stacked satellite velocity disperions for SDSS VAGC. Lastly, Han et al. (2015) use a maximum likelihood weak lensing analysis to fit shapes of SDSS source galaxies individually (unlike the other *stacked* weak lensing analyses) for the G3Cv5 GAMA group catalog**cite**. Each of these works ultimately measure M_h in M_* bins. We derive $\sigma_{\log M_h}$ from the uncertainties in these M_h measurements at M_* bin $\sim 10^{10} M_\odot$. From Mandelbaum et al. (2006b); More et al. (2011); Velander et al. (2014) we have $\sigma_{\log M_h}$ for blue/late-type/star forming centrals while we have $\sigma_{\log M_h}$ for all centrals for Conroy et al. (2007); Han et al. (2015).

The $\sigma_{\log M_h}$ constraints from the literature are significantly scatter from 0.12 to 0.6 dex (right). $\sigma_{\log M_h}$ from our model, regardless of $t_{\rm duty}$ is well within this range, so the comparison does not provide much constraint on $t_{\rm duty}$. Furthermore the $\sigma_{\log M_h}$ are not directly constrained but derived from measurements of M_h. On the other hand, the constraints for $\sigma_{\log M_h}$ in the literature are relatively consistent: $\sigma_{\log M_*} \lesssim 0.2$. Some of these constraints are

from analyses that use halo models that fix $\sigma_{\log M_*}$ as a function of M_h (Leauthaud et al. 2012; Tinker et al. 2013; Zu & Mandelbaum 2015). Such analyses are not ideal measurements of $\sigma_{\log M_*}$ at a specific $M_h \sim 10^{12} M_\odot$. Excluding those analyses, we are left with lower $\sigma_{\log M_*}$ constraints. These constraints are likely even lower, since observational constraints measure the quadratic sum of the intrinsic scatter and measurement scatter.

Based on the $\sigma_{\log M_*}$ comparison, we conclude that our models with longer duty cycles timescales produce scatters too large to reconcile with observations. A short duty cycle timescale, $t_{\rm duty} < 1\,{\rm Gyr}$ is *necessary* for our model to ameliorate the tension with the constraints from literature. However, *even for the shortest duty cycle timescale we probe* ($\sigma_{\log M_*}$ =**number** *for* $t_{\rm duty} = 0.5\,{\rm Gyr}$*), we find some tension in* $\sigma_{\log M_*}$ *between our model and constraints in the literature.*

4.2. The Need for Assembly Bias?

A shorter star formation duty cycle timescale produces smaller scatter in the SHMR of our model. This dependence on the duty cycle timescale, allows us to compare our model with measurements of $\sigma_{\log M_*}$ and $\sigma_{\log M_h}$ to constrain $t_{\rm duty}$, which reflect the star formation variability timescale. Such a comparisons to the literature, in the previous section, demonstrate that $t_{\rm duty} < 1\,{\rm Gyr}$ is necessary to reduce tensions with observed constraints. However, a short duty cycle timescale, alone, is not enough to conservatively reproduce observed $\sigma_{\log M_*}$ constraints. Since our model produces scatter in SHMR larger than observations, the SFR and M_* evolution of the SF centrals in our model need to be more correlated with the accretion histories of their host halos. Therefore, in an effort to better reproduce observed SHMR scatter constraints, in this section, we introduce *assembly bias* into the SFH prescription of our model.

Assembly bias, most commonly in the literature, refers to the dependence of the spatial distribution of dark matter halos on halo properties besides mass (Gao et al. 2005; Wechsler et al. 2006; Gao & White 2007; Wetzel et al. 2007; Li et al. 2008; Sunayama et al. 2016). At low halo mass, older and more concentrated halos form in high density environments. While at high halo mass, the effect is the opposite — younger, less concentrated halos form in high-density regions. Furthermore, as predicted by semi-analytic models (Croton et al. 2007) and found using galaxy group catalogs (Yang et al. 2006; Wang et al. 2008; Tinker et al. 2011; Wang et al. 2013; Lacerna et al. 2014; Tinker et al. 2017a,b, 2018), this assembly bias propagates beyond spatial clustering to galaxy properties such as formation histories and star formation properties. For our model, we incorporate assembly bias by correlating the SFHs of our SF central galaxies with halo growth histories.

More specifically, we correlate the galaxy SFR with respect to the mean SFS SFR (*i.e.* $\Delta \log$ SFR in Eq. 3) to the halo mass accretion over dynamical time. At every $t_{\rm duty}$ timestep, t, $\Delta \log {\rm SFR}(t)$ is assigned based on $\Delta M_h(t) = M_h(t) - M_h(t - t_{\rm dyn}(t))$ in $M_{\rm max}$ bins with

a correlation coefficient r, a parameter added to our model. Our prescription for track halo mass accretion over dynamical time is similar to the Rodríguez-Puebla et al. (2016); Behroozi et al. (2018) empirical models. In Figure 6 we illustrate how we incorporate assembly bias into the SF centrals of our model and the correlation between the host halo accretion history with the SFH with respect to the SFS SFR. We plot the relative halo accretion histories $M_h(t)/M_h(z{=}0.05)$ of two arbitrarily chosen SF centrals with $M_h(z{=}0.05) \sim 10^{12} M_\odot$ in the top panel. Below, we plot $\Delta \log$ SFR, SFH with respect to the SFS, of these galaxies for our model with correlation coefficients $r = 0.5$ and 0.99 (middle and bottom). At some t, we choose a random `TreePM` snapshot (dotted), we can see that $\Delta \log \mathrm{SFR}(t)$ is correlated with halo accretion over the period $t - t_{\rm dyn}$ to t (shaded top panel). The SFHs illustrate the correlation between $\Delta \log \mathrm{SFR}(t)$ and $\Delta M_h = M_h(t) - M_h(t - t_{\rm dyn})$ and how $\Delta \log \mathrm{SFR}(t)$ correlates more with $\Delta M_h(t)$ as r ranges from 0 to 1 (Figure 6).

Next, using our implementation of assembly bias, we compare the model with different values of r to observations using ABC-PMC (see Section 4.1). From the resulting posterior estimates, we examine the scatter in the SHMR ($\sigma_{\log M_*}$) given our model with $r = 0$ (no assembly bias; blue), 0.5 (orange), and 0.99 (green) as a function of $t_{\rm duty}$ in Figure 7. We note that for our model run on the posterior distributions of its parameters reproduce the observed SMF of SF centrals and SFS, for all values of r. At $t_{\rm duty} \geq 5\,\mathrm{Gyr}$ we find no significant difference in $\sigma_{\log M_*}$, regardless of r. Below $t_{\rm duty} < 5\,\mathrm{Gyr}$, however, $\sigma_{\log M_*}$ *of our model decreases significantly with stronger assembly bias in our model.* For $t_{\rm duty} = 0.5\,\mathrm{Gyr}$, we find $\sigma_{\log M_*}$ = **final numbers** for $r = 0., 0.5$, and 0.99, respectively. Comparing our updated model to the constraints included in Figure 5, we find that incorporating assembly bias significantly reduces the tensions with observations (right panel). In fact, with a short star formation duty cycle ($t_{\rm duty} \leq 1\,\mathrm{Gyr}$) and strong assembly bias, our model conservatively reproduces most of the $\sigma_{\log M_*}$ constraints from the literature.

In addition to the observational constraints, we also compare the SHMR scatters of our models to $\sigma_{\log M_*}$ from modern galaxy formation models on the right panel: hydrodynamic simulations (dot filled), semi-analytic models (hatched), and an empirial model (dashed line). For the hydrodynamic simulations, the dotted region encompasses constraints from EAGLE**cite**, Massive Black II**cite**, and Illustris TNG**cite**, as in Figure 8 of Wechsler & Tinker (2018). For the semi-analytic models, the hatched region includes **?**Somerville et al. (2012), and the SAGE model[2]. Finally, we include the empirical model from Behroozi et al. (2018), the UniverseMachine. By varying r and $t_{\rm duty}$, $\sigma_{\log M_*}$ of our model encompasses all of the constraints from galaxy formation models. However, as discussed in Wechsler & Tinker (2018), only the hydrodynamical simulations are in agreement with observations. For short $t_{\rm duty}$ and high r, $\sigma_{\log M_*}$ of our model is in good agreement with the predictions from hydrodynamic simulations.

[2] https://tao.asvo.org.au/tao/

A key element of our model is the SFH prescription for SF central galaxies where the SFH evolves about the SFS. Contrary to our SFH prescription, **?**, for example, argue that the SFS is a simple consequence of central limit theorem and can be reproduced even if *in situ* stellar mass growth is modeled as a stochastic process like a random walk. Gladders et al. (2013); Abramson et al. (2015, 2016), similarly argue that ~ 2000 loosely constrained log-normal SFHs can reproduce observations such as the SMF at $z \leq 8$ and the SFS at $z \leq 6$. These works, however, focus on reproducing galaxy observations and do not examine the galaxy-halo connection such as the SHMR. In order to test whether log-normal SFHs can also produce realistic SHMRs, we take the SFHs (SFR(t) and $M_*(t)$) from Abramson et al. (2016) and assign them to halos by abundance matching their M_* to M_h at $z{\sim}1$. We then restrict the SFHs to those that would be classified as star-forming based on a rough log SSFR > -11. cut. Afterwards we measure $\sigma_{\log M_*}$ at the lowest M_h where it can be reliably measured given the Abramson et al. (2016) sample $M_*{>}10^{10} M_\odot$ limit: $\sigma_{\log M_*}(M_h = 10^{12.4}) = 0.33 \pm 0.04$ (dotted line in Figure 7). Although the Abramson et al. (2016) SFHs can reproduce galaxy observations, $\sigma_{\log M_*}$ derived from the SFHs and abundance matching have significant tension with observational constraints and predictions from hydrodynamic simulations. This estimate is, however, derived from a simple abundance matching scheme. As Diemer et al. (2017) find from their log-normal fits to the SFHs of Illustris galaxies, halo formation history correlates with the fits. Incorporating such assembly bias into our abundancing matching may reduce $\sigma_{\log M_*}$.

In this section, we demonstrate that incorporating assembly bias into our model by correlating ΔSFR to ΔM_h reduces the tension with the SHMR scatter in observations. With assembly bias added, our model can produce the range of $\sigma_{\log M_*}$ constraints from observations as well as modern galaxy formation models. More importantly, a short star formation duty cycle timescale ($\lesssim 1$ Gyr) and strong assembly bias $r > 0.5$ is necessary to conservatively reproduce current observational constraints.

5. Summary and Conclusion

A. $z \sim 1$ Initial Conditions

Much of the results presented in this paper are based on comparison between our model and observations at $z \sim 0$.. Our model is initalized at $z \sim 1$. Therefore, in this section we test some of the choices we make in our intializations.

- Test impact of $z \sim 1$ SMF
- Test impact of $z \sim 1$ $\sigma_{\log M_*}$

Acknowledgements

It's a pleasure to thank Louis Abramson, Shy Genel, **more acknowledgements** for valueable discussions.

REFERENCES

Abazajian, K. N., Adelman-McCarthy, J. K., Agüeros, M. A., et al. 2009, The Astrophysical Journal Supplement Series, 182, 543

Abramson, L. E., Gladders, M. D., Dressler, A., et al. 2016, The Astrophysical Journal, 832, 7

—. 2015, The Astrophysical Journal Letters, 801, L12

Alsing, J., Wandelt, B., & Feeney, S. 2018, arXiv:1801.01497 [astro-ph], arXiv:1801.01497 [astro-ph]

Baldry, I. K., Balogh, M. L., Bower, R. G., et al. 2006, Monthly Notices of the Royal Astronomical Society, 373, 469

Behroozi, P., Wechsler, R., Hearin, A., & Conroy, C. 2018, arXiv:1806.07893 [astro-ph], arXiv:1806.07893 [astro-ph]

Blanton, M. R., & Moustakas, J. 2009, Annual Review of Astronomy and Astrophysics, 47, 159

Blanton, M. R., & Roweis, S. 2007, The Astronomical Journal, 133, 734

Blanton, M. R., Schlegel, D. J., Strauss, M. A., et al. 2005, The Astronomical Journal, 129, 2562

Brinchmann, J., Charlot, S., White, S. D. M., et al. 2004, Monthly Notices of the Royal Astronomical Society, 351, 1151

Campbell, D., van den Bosch, F. C., Hearin, A., et al. 2015, Monthly Notices of the Royal Astronomical Society, 452, 444

Chabrier, G. 2003, Publications of the Astronomical Society of the Pacific, 115, 763

Conroy, C., Wechsler, R. H., & Kravtsov, A. V. 2006, The Astrophysical Journal, 647, 201

Conroy, C., Prada, F., Newman, J. A., et al. 2007, The Astrophysical Journal, 654, 153

Croton, D. J., Gao, L., & White, S. D. M. 2007, Monthly Notices of the Royal Astronomical Society, 374, 1303

Daddi, E., Dickinson, M., Morrison, G., et al. 2007, The Astrophysical Journal, 670, 156

Davis, M., Efstathiou, G., Frenk, C. S., & White, S. D. M. 1985, The Astrophysical Journal, 292, 371

Diemer, B., Sparre, M., Abramson, L. E., & Torrey, P. 2017, The Astrophysical Journal, 839, 26

Drory, N., Bundy, K., Leauthaud, A., et al. 2009, The Astrophysical Journal, 707, 1595

Gao, L., Springel, V., & White, S. D. M. 2005, Monthly Notices of the Royal Astronomical

Society, 363, L66
Gao, L., & White, S. D. M. 2007, Monthly Notices of the Royal Astronomical Society, 377, L5
Genel, S., Vogelsberger, M., Springel, V., et al. 2014, Monthly Notices of the Royal Astronomical Society, 445, 175
Gladders, M. D., Oemler, A., Dressler, A., et al. 2013, The Astrophysical Journal, 770, 64
Hahn, C., Tinker, J. L., & Wetzel, A. R. 2017a, The Astrophysical Journal, 841, 6
Hahn, C., Vakili, M., Walsh, K., et al. 2017b, Monthly Notices of the Royal Astronomical Society, 469, 2791
Hahn, C., Blanton, M. R., Moustakas, J., et al. 2015, The Astrophysical Journal, 806, 162
Han, J., Eke, V. R., Frenk, C. S., et al. 2015, Monthly Notices of the Royal Astronomical Society, 446, 1356
Ilbert, O., McCracken, H. J., Le Fèvre, O., et al. 2013, Astronomy and Astrophysics, 556, A55
Karim, A., Schinnerer, E., Martínez-Sansigre, A., et al. 2011, The Astrophysical Journal, 730, 61
Lacerna, I., Padilla, N., & Stasyszyn, F. 2014, Monthly Notices of the Royal Astronomical Society, 443, 3107
Leauthaud, A., Tinker, J., Bundy, K., et al. 2012, The Astrophysical Journal, 744, 159
Lee, N., Sanders, D. B., Casey, C. M., et al. 2015, The Astrophysical Journal, 801, 80
Leja, J., van Dokkum, P., & Franx, M. 2013, The Astrophysical Journal, 766
Li, C., & White, S. D. M. 2009, Monthly Notices of the Royal Astronomical Society, 398, 2177
Li, Y., Mo, H. J., & Gao, L. 2008, Monthly Notices of the Royal Astronomical Society, 389, 1419
Magdis, G. E., Daddi, E., Béthermin, M., et al. 2012, The Astrophysical Journal, 760, 6
Mamon, G. A., Sanchis, T., Salvador-Solé, E., & Solanes, J. M. 2004, Astronomy and Astrophysics, 414, 445
Mandelbaum, R., Seljak, U., Cool, R. J., et al. 2006a, Monthly Notices of the Royal Astronomical Society, 372, 758
Mandelbaum, R., Seljak, U., Kauffmann, G., Hirata, C. M., & Brinkmann, J. 2006b, Monthly Notices of the Royal Astronomical Society, 368, 715
Marchesini, D., van Dokkum, P. G., Förster Schreiber, N. M., et al. 2009, The Astrophysical Journal, 701, 1765
More, S., van den Bosch, F. C., Cacciato, M., et al. 2011, Monthly Notices of the Royal Astronomical Society, 410, 210
Moustakas, J., Coil, A. L., Aird, J., et al. 2013, The Astrophysical Journal, 767, 50
Muzzin, A., Marchesini, D., Stefanon, M., et al. 2013, The Astrophysical Journal, 777, 18

Noeske, K. G., Weiner, B. J., Faber, S. M., et al. 2007, The Astrophysical Journal Letters, 660, L43

Peng, Y.-j., Lilly, S. J., Kovač, K., et al. 2010, The Astrophysical Journal, 721, 193

Rodríguez-Puebla, A., Primack, J. R., Behroozi, P., & Faber, S. M. 2016, Monthly Notices of the Royal Astronomical Society, 455, 2592

Salim, S., Rich, R. M., Charlot, S., et al. 2007, The Astrophysical Journal Supplement Series, 173, 267

Santini, P., Fontana, A., Grazian, A., et al. 2009, Astronomy and Astrophysics, 504, 751

Somerville, R. S., Gilmore, R. C., Primack, J. R., & Domínguez, A. 2012, Monthly Notices of the Royal Astronomical Society, 423, 1992

Speagle, J. S., Steinhardt, C. L., Capak, P. L., & Silverman, J. D. 2014, The Astrophysical Journal Supplement Series, 214, 15

Sunayama, T., Hearin, A. P., Padmanabhan, N., & Leauthaud, A. 2016, Monthly Notices of the Royal Astronomical Society, 458, 1510

Tinker, J., Wetzel, A., & Conroy, C. 2011, ArXiv e-prints, 1107, arXiv:1107.5046

Tinker, J. L., Hahn, C., Mao, Y.-Y., & Wetzel, A. R. 2017a, arXiv:1705.08458 [astro-ph], arXiv:1705.08458 [astro-ph]

Tinker, J. L., Hahn, C., Mao, Y.-Y., Wetzel, A. R., & Conroy, C. 2018, Monthly Notices of the Royal Astronomical Society, 477, 935

Tinker, J. L., Leauthaud, A., Bundy, K., et al. 2013, The Astrophysical Journal, 778, 93

Tinker, J. L., Wetzel, A. R., Conroy, C., & Mao, Y.-Y. 2017b, Monthly Notices of the Royal Astronomical Society, 472, 2504

Vale, A., & Ostriker, J. P. 2006, Monthly Notices of the Royal Astronomical Society, 371, 1173

Velander, M., van Uitert, E., Hoekstra, H., et al. 2014, Monthly Notices of the Royal Astronomical Society, 437, 2111

Vogelsberger, M., Genel, S., Springel, V., et al. 2014, Monthly Notices of the Royal Astronomical Society, 444, 1518

Wang, L., Farrah, D., Oliver, S. J., et al. 2013, Monthly Notices of the Royal Astronomical Society, 431, 648

Wang, Y., Yang, X., Mo, H. J., et al. 2008, The Astrophysical Journal, 687, 919

Wechsler, R. H., & Tinker, J. L. 2018, ArXiv e-prints, 1804, arXiv:1804.03097

Wechsler, R. H., Zentner, A. R., Bullock, J. S., Kravtsov, A. V., & Allgood, B. 2006, The Astrophysical Journal, 652, 71

Wetzel, A. R., Cohn, J. D., & White, M. 2009, Monthly Notices of the Royal Astronomical Society, 395, 1376

Wetzel, A. R., Cohn, J. D., White, M., Holz, D. E., & Warren, M. S. 2007, The Astrophysical Journal, 656, 139

Wetzel, A. R., Tinker, J. L., & Conroy, C. 2012, Monthly Notices of the Royal Astronomical Society, 424, 232

Wetzel, A. R., Tinker, J. L., Conroy, C., & van den Bosch, F. C. 2013, Monthly Notices of the Royal Astronomical Society, 432, 336

—. 2014, Monthly Notices of the Royal Astronomical Society, 439, 2687

Wetzel, A. R., & White, M. 2010, Monthly Notices of the Royal Astronomical Society, 403, 1072

Whitaker, K. E., van Dokkum, P. G., Brammer, G., & Franx, M. 2012, The Astrophysical Journal Letters, 754, L29

White, M. 2002, The Astrophysical Journal Supplement Series, 143, 241

White, M., Cohn, J. D., & Smit, R. 2010, Monthly Notices of the Royal Astronomical Society, 408, 1818

Yang, X., Mo, H. J., & van den Bosch, F. C. 2006, The Astrophysical Journal Letters, 638, L55

—. 2009, The Astrophysical Journal, 695, 900

Yang, X., Mo, H. J., van den Bosch, F. C., & Jing, Y. P. 2005, Monthly Notices of the Royal Astronomical Society, 356, 1293

Zu, Y., & Mandelbaum, R. 2015, Monthly Notices of the Royal Astronomical Society, 454, 1161

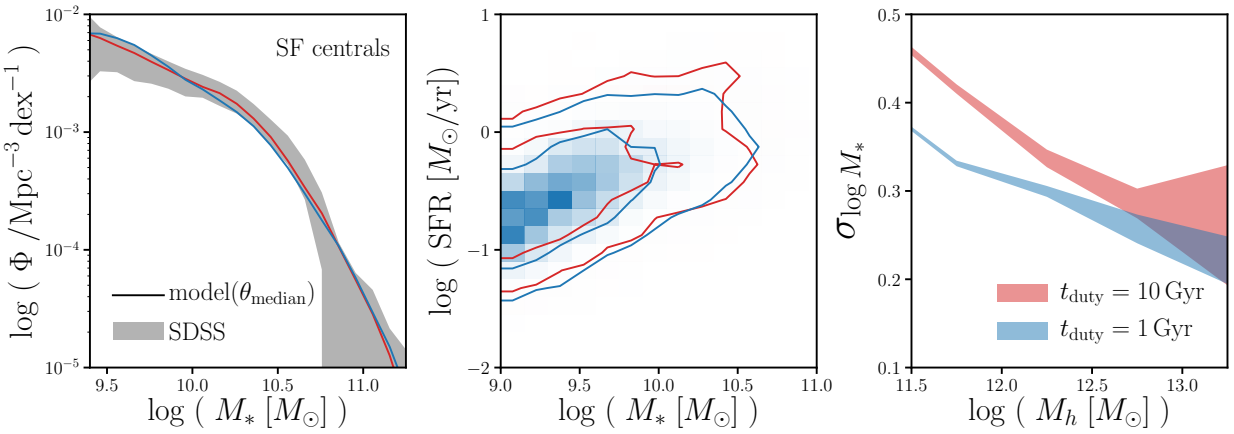

Fig. 4.— Our models with different star formation duty cycle timescales (blue: $t_{\rm duty}$=1 Gyr; red: $t_{\rm duty}$=10 Gyr) run with median values of their ABC posterior distribution have SMFs and SFSs consistent with observations (left and middle). *They however produce significantly different scatter in* log M_* *at fixed* log $M_{\rm halo}$ *— scatter in the SHMR (right).* By comparing the scatter in SHMR of our models to observational constraints on the SHMR, we constrain the timescale of the star formation duty cycle and thereby the SFHs of star forming galaxies.

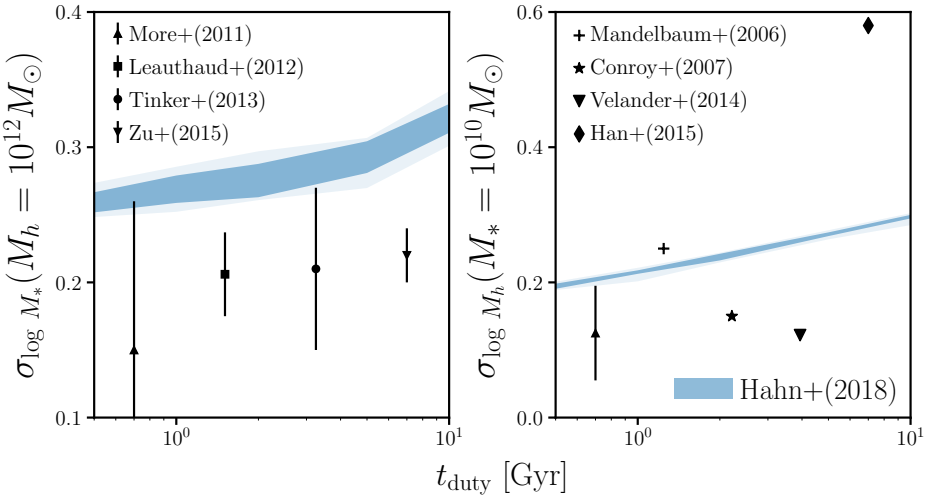

Fig. 5.— With shorter star formation duty cycle timescales, $t_{\rm duty}$, our model produces smaller scatter in the SHMR—$\sigma_{\log M_*}$ at M_h=$10^{12} M_\odot$ (left) and $\sigma_{\log M_h}$ at M_*=$10^{10} M_\odot$. For $t_{\rm duty}$ = 10 Gyr, $\sigma_{\log M_*}$ = 0.32 dex and $\sigma_{\log M_h}$ = 0.30 dex. Meanwhile for $t_{\rm duty}$ = 0.5 Gyr, $\sigma_{\log M_*}$ = 0.26 dex and $\sigma_{\log M_h}$ = 0.20. We include $\sigma_{\log M_*}$ constraints from Yang et al. (2009); More et al. (2011); Leauthaud et al. (2012); Tinker et al. (2013); Zu & Mandelbaum (2015) and $\sigma_{\log M_h}$ constraints from Mandelbaum et al. (2006a); Conroy et al. (2007); More et al. (2011); Velander et al. (2014); Han et al. (2015) (see text). The Mandelbaum et al. (2006a); Han et al. (2015) $\sigma_{\log M_h}$ constraints serve as upper limits. A short star formation duty cycle timescale is necessary to produce a tight SHMR roughly consistent with constraints from observations.

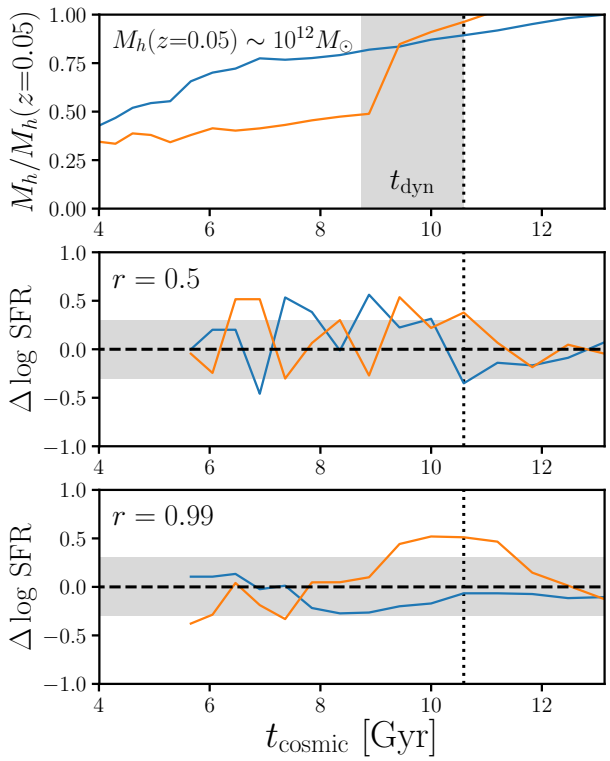

Fig. 6.— We incorporate assembly bias into the SF centrals of our model by correlating host halo accretion history with the SFH with respect to the SFS SFR. We plot the relative halo accretion history, $M_h(t)/M_h(z{=}0.05)$ for two arbitrarily chosen SF centrals with $M_h(z{=}0.05) \sim 10^{12} M_\odot$, in the top panel. In the two panels below we present $\Delta \log$ SFR, SFH with respect to the SFS, of these galaxies for our model with correlation coefficients $r = 0.5$ and 0.99 (middle and bottom). At some t (dotted), $\Delta \log \mathrm{SFR}(t)$ is correlated with halo accretion over the range $t - t_{\rm dyn}$ to $t_{\rm dyn}$ (shaded top panel). The SFHs illustrate how $\Delta \log \mathrm{SFR}(t)$ correlates with $\Delta M_h = M_h(t) - M_h(t - t_{\rm dyn})$ and with stronger correlations for larger r.

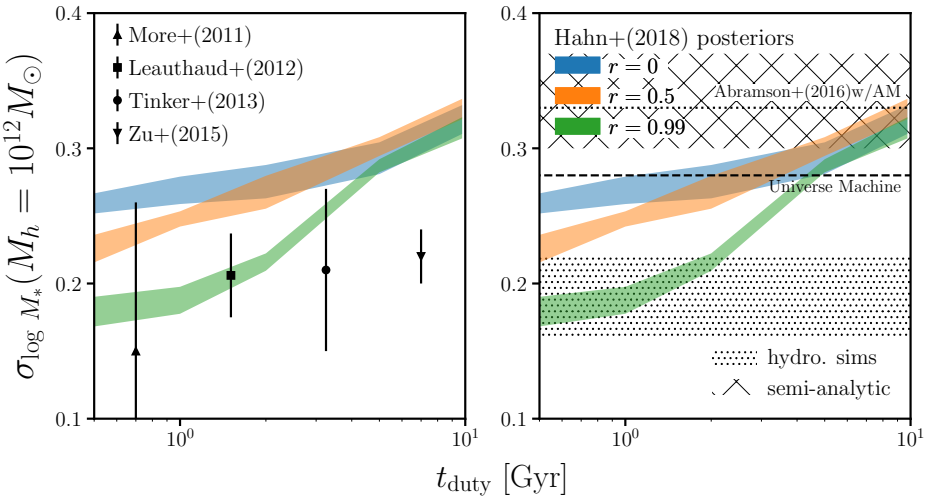
More+(2011)
Leauthaud+(2012)
Tinker+(2013)
Zu+(2015)
Hahn+(2018) posteriors
$r = 0$
$r = 0.5$
$r = 0.99$
Abramson+(2016)w/AM
Universe Machine
hydro. sims
semi-analytic
$\sigma_{\log M_*}(M_h = 10^{12} M_\odot)$
$t_{\rm duty}$ [Gyr]
0.1
0.2
0.3
0.4
10^0
10^1

Fig. 7.—